Mon. Not. R. Astron. Soc. **352,** L35–L39 (2004) doi:10.1111/j.1365-2966.2004.08163.x

Gamma-ray bursts from synchrotron self-Compton emission

Boris E. Stern[1,2,3★] and Juri Poutanen[1★†]

[1]*Astronomy Division, PO Box 3000, 90014 University of Oulu, Finland*
[2]*Institute for Nuclear Research, Russian Academy of Sciences, 7a, Prospect 60-letija Oktjabrja, Moscow 117312, Russia*
[3]*Astro Space Center of Lebedev Physical Institute, Profsoyuznaya 84/32, Moscow 117997, Russia*

Accepted 2004 June 28. Received 2004 June 25; in original form 2004 May 25

ABSTRACT

The emission mechanism of gamma-ray bursts (GRBs) is still a matter of debate. The standard synchrotron energy spectrum of cooling electrons $F_E \propto E^{-1/2}$ is much too soft to account for the majority of the observed spectral slopes. An alternative in the form of quasi-thermal Comptonization in a high-compactness source has difficulties in reproducing the peak of the observed photon distribution below a few hundred keV. We show here that for typical parameters expected in the GRB ejecta the observed spectra in the 20–1000 keV energy range can be produced by inverse Compton scattering of the synchrotron radiation in a partially self-absorbed regime. If the particles are continuously accelerated/heated over the lifetime of a source rather than being instantly injected, a prominent peak develops in their distribution at a Lorentz factor $\gamma \sim 30$–100, where synchrotron and inverse-Compton losses are balanced by acceleration and heating due to synchrotron self-absorption. The synchrotron peak should be observed at 10–100 eV, whereas the self-absorbed low-energy tail with $F_E \propto E^2$ can produce the prompt optical emission (as in the case of GRB 990123). The first Compton scattering radiation by nearly monoenergetic electrons can then be as hard as $F_E \propto E^1$, reproducing the hardness of most of the observed GRB spectra. The second Compton peak should be observed in the high-energy gamma-ray band, possibly being responsible for the 10–100 MeV emission detected in GRB 941017. A significant electron–positron pair production reduces the available energy per particle, moving the spectral peaks to lower energies as the burst progresses. The regime is very robust, operates in a broad range of parameter space and can explain most of the observed GRB spectra and their temporal evolution.

Key words: radiation mechanisms: non-thermal – scattering – methods: numerical – gamma-rays: bursts – gamma-rays: theory.

1 INTRODUCTION

Spectra of the prompt soft gamma-ray emission of gamma-ray bursts (GRBs) are still not explained and seem mysterious despite large theoretical efforts devoted to this problem. Already in the 1980s it was recognized that synchrotron emission from the electrons injected at high energies produces cooling spectra $F_E \propto E^{-1/2}$ (described by a photon spectral index $\alpha = -3/2$) which are much too soft to be consistent with that observed from GRBs (e.g. Bussard 1984; Imamura & Epstein 1987). The problem became acute when Preece et al. (2000) showed that the time-resolved spectra have the mean observed α close to -1 (i.e. $F_E \propto E^0$) and some spectra can be as hard as $F_E \propto E^1$. In spite of these facts, many different versions of the synchrotron shock models were proposed recently (see, for example, Tavani 1996; Chiang & Dermer 1999; Piran 1999) to explain GRB spectra. Panaitescu & Mészáros (2000) hypothesized that inverse Compton scattering of synchrotron self-absorbed radiation can be responsible for the hard spectra, observed by the Burst and Transient Source Experiment (BATSE) in the 20–1000 keV range, under an assumption that electrons emit in a *slow* cooling regime, which, however, is hardly possible in the GRB ejecta (Ghisellini & Celotti 1999; Ghisellini, Celotti & Lazzati 2000).

In principle, efficient cooling of electrons can be prevented by their reacceleration (Lloyd & Petrosian 2000). In synchrotron models, this requires the fraction of particles taking part in that process to be orders of magnitudes smaller than the total number of particles (not to exceed the available energy) and these particles should always be the same (Ghisellini et al. 2000), conditions that are difficult to imagine.

Problems with the relativistic synchrotron (and self-Compton) models gave rise to optically thick emission models such as quasi-thermal Comptonization (Zdziarski & Lamb 1986; Thompson 1994; Liang 1997; Ghisellini & Celotti 1999; Stern 1999), where the

★E-mail: stern@bes.asc.rssi.ru (BES); juri.poutanen@oulu.fi (JP)
†Corresponding Fellow, NORDITA, Copenhagen.

energy is shared among many particles which are now mildly relativistic. If the synchrotron radiation is self-absorbed, one can achieve rather hard spectra with the peak at 10–50 keV in the comoving frame of the ejecta. For the bulk Lorentz factor $\Gamma \sim 100$, this peak shifts, however, to an uncomfortably high energy.

In this paper we show that optically thin synchrotron self-Compton mechanism operating at parameters expected in the GRB ejecta can naturally produce very hard spectra peaking in the BATSE energy band, if the available energy is shared among all particles and the particles are continuously accelerated/heated over the lifetime of a source. In such conditions, the electron/pair distribution develops a prominent peak at a Lorentz factor $\gamma \sim 30$–100, where synchrotron and Compton losses are balanced by particle acceleration and heating due to synchrotron self-absorption. Copious pair production reduces available energy per particle, moving the spectral peak to lower energies as the burst progresses, reproducing thus the hard-to-soft evolution observed in time-resolved spectra (Ford et al. 1995; Ryde & Svensson 2002). High-energy emission observed in some GRBs (e.g. GRB 941017, González et al. 2003) and the prompt optical emission observed in GRB 990123 (Akerlof et al. 1999) can also be explained in this model simultaneously.

2 MAIN PARAMETERS

Let us consider the ejecta moving with Lorentz factor Γ at the distance R from the source. The main parameters determining radiation physics are the (comoving) energy dissipation rate, magnetic field strength B, size of the emission region R' and the number of particles described by the Thomson optical depth $\tau_{\rm T} = n_{\rm e} R' \sigma_{\rm T}$. It is suitable to describe the available energy by the comoving compactness

$$\Lambda = \frac{U}{m_{\rm e}c^2} R' \sigma_{\rm T}, \tag{1}$$

where U is the comoving density of a relevant kind of energy. Formally, Λ is just the optical depth $\tau_{\rm T}$ of pairs if we would spend all available energy for their mass. In reality, most energy goes to radiation and the resulting $\tau_{\rm T} \ll \Lambda$ (e.g. $\tau_{\rm T} \sim 10$–20 at $\Lambda = 10^3$ and $\tau_{\rm T} \sim 1$ at $\Lambda = 30$). The role of magnetic fields can be described by the magnetic compactness $\Lambda_{\rm B}$ given by equation (1) with $U = B^2/(8\pi)$. The ratio $\Lambda_{\rm B}/\Lambda$ is model-dependent. We assume that the magnetic field is below equipartition, i.e. $\Lambda_{\rm B} \lesssim \Lambda$. Even in magnetically dominating models, one does not expect that $\Lambda_{\rm B} \gg \Lambda$ necessarily, because reconnection of magnetic field providing the energy dissipation can reduce its strength *within* the emission region to $\Lambda_{\rm B} \sim \Lambda$.

It is evident that R' should not exceed the size of the causally connected region, i.e. R/Γ in both transversal and radial directions (the latter in the observer's frame is R/Γ^2). We assume that $R' = R/\Gamma$ and measure the comoving time t' in units of the light crossing time of the region $R'/c = R/(c\Gamma)$ which corresponds to the observer time $R/(c\Gamma^2)$. The dissipation compactness (corresponding to the energy dissipation *rate*) is then $\ell = {\rm d}\Lambda/{\rm d}t'$. (For a constant dissipation rate during $t' = 1$ we get $\ell = \Lambda$.) It can be estimated from the observed isotropic energy release $E_{\rm rad}$ assuming that the energy was dissipated homogeneously in a causally connected region

$$\ell = \frac{E_{\rm rad}\sigma_{\rm T}}{m_{\rm e}c^2 \Gamma 4\pi R^2} = 7\, E_{\rm rad,52} \Gamma_2^{-1} R_{15}^{-2}. \tag{2}$$

(Here we adopt notation $Q = 10^x Q_x$ in cgs units if not mentioned otherwise.) Fig. 1 demonstrates the levels of the compactness and the observed time-scale on a R–Γ plane. The observed emission episode at first glance should be a single pulse of time-scale $R/(c\Gamma^2)$.

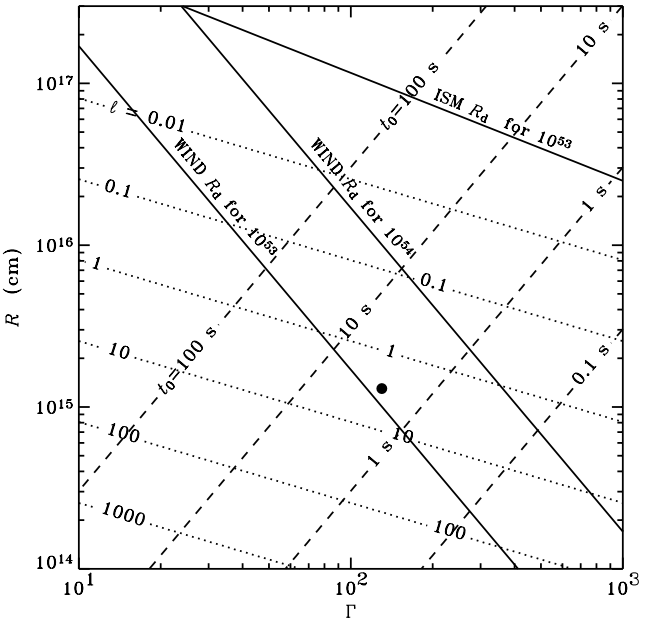

Figure 1. The map of Γ–R parameter space. The dotted lines show constant compactness ℓ levels for energy release $E_{\rm rad} = 10^{52}$ erg in the causally connected region given by equation (2). The dashed lines show the time-scale in the observer frame defined as $t_0 = R/(c\Gamma^2)$. The deceleration limit $R_{\rm d}$ for different $E_{\rm K}$ is given for the wind with the mass-loss rate 10^{-5} $M_\odot$ yr^{-1} and velocity of 10^3 km s^{-1} as well as for the interstellar medium of $n_{\rm ISM} = 1$ cm^{-3} (see equation [3]). The circle corresponds to the model run simulated in the paper.

Actually, most GRBs have a complex time structure. We can then prescribe this episode to a single GRB pulse and associate $E_{\rm rad}$ with its energy fluence, or admit that the energy can be released by compact flares within the causally connected region. In that case, $E_{\rm rad}$ should be referred to the fluence of a complex emission episode and equation (2) then gives an average compactness in the region, whereas the local values of ℓ can be substantially higher.

What is the typical size R where the energy dissipation takes place? For radii $\lesssim 10^{14}$ cm, the compactness is large, $\ell \gtrsim 300$ (see Fig. 1), pair production is extremely efficient and the mean energy available per particle is rather small. The main emission mechanism is then multiple Compton scattering. The spectra expected from this regime can be hard (Ghisellini & Celotti 1999; Stern 1999), but peaked at too high energies (10–50 keV in the comoving frame). At $R \gtrsim 10^{15}$ cm, the compactness and optical depth are smaller, and the mean energy available per particle larger and the energy is radiated away by optically thin synchrotron or synchrotron self-Compton emission.

The dissipation radius is also limited from above by deceleration of ejecta in the external environment:

$$R_{\rm d} \sim \begin{cases} 1.7 \times 10^{16}\ E_{\rm K,54}\ w_3 \dot{M}_{-5}^{-1} \Gamma_2^{-2}\ {\rm cm} & \text{for wind,} \\ 2.5 \times 10^{17}\ E_{\rm K,54}^{1/3} n_{\rm ISM}^{-1/3} \Gamma_2^{-2/3}\ {\rm cm} & \text{for ISM,} \end{cases} \tag{3}$$

where the ejecta sweeps up mass $\sim M_{\rm ej}/\Gamma$ (see solid lines in Fig. 1). Here $E_{\rm K} = \Gamma\ M_{\rm ej} c^2$ is the isotropic kinetic energy of the ejecta, $n_{\rm ISM}$ cm^{-3} is particle concentration in the interstellar medium, $\dot{M}_{-5}$ is the mass-loss rate by the progenitor star in units of 10^{-5} $M_\odot$ yr^{-1} and w_3 is the wind velocity in units of 1000 km s^{-1}. We notice that the deceleration limit in the wind case restricts the low compactness ($\ell \lesssim 10$) regime to a relatively narrow region of parameters. If the kinetic energy is $\lesssim 10^{53}$ erg, or if the environment is denser, then the

low-compactness regime is hardly possible at all. Thus we consider the typical dissipation radius $R = 10^{15}$ cm. The observed pulse duration of about 1 s is consistent with the fact that GRBs have very little power at time-scales below 1 s (Beloborodov, Stern & Svensson 2000).

The optical depth τ_T in the emission region is bounded from above by the opacity of the ejecta

$$\tau_{ej} = 0.3\, E_{K,54}\, R_{15}^{-2}\, \Gamma_2^{-1} \tag{4}$$

(assuming matter-dominated ejecta and that the matter is concentrated within a causally connected shell). For external shocks, τ_T cannot be smaller than that determined by collected material

$$\tau_{ext} = \begin{cases} 2\times 10^{-4}\, \dot{M}_{-5}\, R_{15}^{-1}\, w_3^{-1} & \text{for wind,} \\ 2\times 10^{-8}\, R_{17}\, n_{ISM} & \text{for ISM.} \end{cases} \tag{5}$$

What is the physical mechanism of the energy dissipation? In the external shock models (Rees & Mészáros 1992; Piran 1999), the dissipation occurs at $R \sim R_d$, which can be about 10^{15} cm for the wind environment if $E_K \sim 10^{53}$ erg and $\Gamma \sim 200$ (see Fig. 1). The impulsive first-order Fermi acceleration would operate in a fast cooling regime (see Stern 2003 for a specific version of this scenario) which, as discussed in the Introduction, contradicts the data. An alternative version of shock energy dissipation is particle heating by plasma instabilities behind the shock front (see, for example, Frederiksen et al. 2003). We follow this route here. It can also operate in internal or 'refreshed' shocks, which could be produced by collisions of fresh ejecta with previously ejected, partially decelerated material. In the Poynting-flux-dominated models (Usov 1994; Lyutikov & Blandford 2003), the magnetic field energy can be dissipated at the required distances.

3 PHYSICAL MODEL

3.1 Model setup

As we have seen, a number of models can satisfy our requirements. Thus we do not specify the exact model for the energy dissipation, but consider a toy model where energy is injected to the emission region with the constant rate during comoving time R'/c. We adopt a slab geometry of the emission region which, in a zero approximation, is consistent with both internal and external shock scenarios. Indeed, we can expect that the main energy release takes place behind the shock front in a layer which is thin relative to the size of the causally connected region. This geometry can also be a satisfactory approximation for the magnetic reconnection scenario. Indeed, the magnetic field is probably predominantly transversal and the reconnection plane is again perpendicular to the direction of propagation.

We neglect the curvature of the shock front and the bulk velocity gradient, thus reducing the problem to a static slab. In this approach we omit a number of effects associated with relativistic expansion of the emitting shell. These effects are important for the description of the time evolution; however, they are not critical for understanding general spectral properties. The thickness of the emitting slab, $\Delta < 1$ (in units of R'), is unknown because it depends on the relaxation process behind the shock front and is probably smaller in the case of the reconnection scenario. We take $\Delta = 0.1$, but the results are not very sensitive to its value.

The energy release is uniform over the slab volume and we assume that the energy is injected in a form of acceleration of electrons and pairs which obtain equal amount of energy per unit time. The optical depth can increase due to pair production. We treat the magnetic field geometry as chaotic, therefore all pairs are isotropic.

The model is fully described by four parameters: (i) the initial Thomson optical depth across the slab, $\tau_0 = n_e \sigma_T \Delta R'$; (ii) the comoving size R'; (iii) the dissipation compactness ℓ; and (iv) the magnetic compactness Λ_B.

3.2 Radiative processes

Let us first consider how particles (electron and positrons) of Lorentz factor γ are heated and how they cool. The energy gain rate of a particle is simply given by the heating rate $\propto \ell$ divided by the number of particles (which is proportional to the total Thomson optical depth, including pairs, across the slab, τ_T). Particles cool by emitting synchrotron radiation and by scattering this radiation (self-Compton mechanism). The energy balance equation can be written as

$$\frac{d\gamma}{dt'} = \frac{\ell}{\tau_T} - \frac{4}{3}(\eta\Lambda_B + \Lambda_T)\gamma^2. \tag{6}$$

Here $\eta < 1$ accounts for the reduced synchrotron cooling due to synchrotron self-absorption, and Λ_T is the compactness corresponding to the energy density of soft photons in the Thomson regime (with energy $\epsilon \equiv E/m_e c^2 \lesssim 1/\gamma$). The typical cooling time is then $t_{cool} \sim 1/[(\Lambda_T + \eta\Lambda_B)\,\gamma]$, which, for the GRB conditions, is orders of magnitude smaller than the light-crossing time.

The balance between heating and cooling is achieved at

$$\gamma_b \approx \sqrt{\ell/(\Lambda_T + \eta\Lambda_B)}\,\tau_T^{-1/2}, \tag{7}$$

where Λ_T and η also depend on γ_b. Particles with $\gamma > \gamma_b$ lose energy faster than they gain it, while at $\gamma < \gamma_b$ the situation is opposite. As a result, a very narrow electron distribution peaked at γ_b develops. This allows us to adopt the approximation that all particles have the same Lorentz factor $\gamma = \gamma_b$. The radiation compactness Λ_T can be expressed as a sum of the synchrotron $\Lambda_s = y\eta\Lambda_B$ and first Compton scattering $\Lambda_c = y\eta\Lambda_s$ energy densities (further scattering orders are in the Klein–Nishina limit). In the adopted approximation, the Compton parameter is just $y = \xi\tau_T\gamma^2$, where the geometrical factor $\xi \sim 1$ for a spherical source and $\xi \sim (2/3)\ln(3/2\Delta) \sim 1.8$ for a slab with $\Delta = 0.1$. Thus equation (7) is reduced to

$$y(1 + y + y^2) \approx \xi\ell/(\eta\Lambda_B). \tag{8}$$

When synchrotron self-absorption is negligible, $\eta = 1$, we find the solution $y_0 \approx (\xi\ell/\Lambda_B)^{1/3}$ (or $y_0 \approx (\xi\ell/\Lambda_B)^{1/2}$, if the second Compton scattering operates close to the Klein–Nishina limit). At small η, Compton parameter increases.

The importance of self-absorption depends crucially on γ. The optical depth at frequencies below the synchrotron emission peak is (equation 2.18a in Ghisellini & Svensson 1991)

$$\tau_s = 15\tau_T/(b\gamma^5 x^{5/3}), \qquad x = \epsilon/(3\gamma^2 b), \tag{9}$$

where $b = B/B_{QED}$ and $B_{QED} = 4.4\times 10^{13}$ G. Thus the emission will be significantly reduced if the self-absorption frequency (where $\tau_s = 1$) is above the emission peak ($x \gtrsim 1$). This happens at $\gamma < \gamma_{cr} = 50\,(\tau_{T,-3}/B_3)^{1/5}$. The same condition for τ_T expressed via the Compton parameter is $\tau_T > \tau_{cr}(y) = 0.5\times 10^{-3}(y/\xi)^{5/7} B_3^{2/7}$.

We now can predict the temporal evolution of the radiation spectrum. The optical depth starts growing after about two light-crossing times 2Δ required to produce high-energy photons. If $\tau_T < \tau_{cr}(y_0)$, the synchrotron is not absorbed, $y = y_0$, $\gamma^2 = y_0/(\xi\tau_T)$ and the synchrotron peak energy decreases with optical depth as $\epsilon_s \sim 3\gamma^2 b \sim 2\times 10^{-7}(y_0/\xi)^{2/7} B_3^{5/7}\tau_{cr}/\tau_T$. The first Compton peak evolves even faster: $\epsilon_{c1} \sim (4/3)\,\gamma^2\,\epsilon_s \sim 4\times 10^{-4}(y_0/\xi)^{4/7} B_3^{3/7}(\tau_{cr}/\tau_T)^2$. When τ_T grows above τ_{cr}, η decreases because of self-absorption, y correspondingly increases (equation 8), the synchrotron peak becomes more stable, and the resulting electron energy and the first

Compton peak start to evolve slower. The second Compton peak is produced in the Klein–Nishina limit at small τ_T, and evolves slowly, $\epsilon_{c2} \sim \gamma \propto 1/\sqrt{\tau_T}$, whereas at larger τ_T the evolution speeds up. We now check these predictions by numerical simulations.

3.3 Simulations

The simulations were performed using a Large Particle Monte Carlo code (LPMC) developed by Stern (1985) and Stern et al. (1995). It handles Compton scattering, photon–photon pair production and pair annihilation, synchrotron radiation and synchrotron self-absorption. Exact cross-sections are used for the first three processes, while the cross-sections in the relativistic approximation are used for the synchrotron process (Ghisellini & Svensson 1991). The electron/pair and photon distributions are computed self-consistently. The code is essentially non-linear: the simulated particles constitute at the same time a target medium for other particles. The geometry of the emission region is a pillbox of radius R' and thickness $\Delta = 0.1$. Output photons are recorded when they cross the surfaces $z = \pm(\Delta/2 + 0.1)R'$.

As an example, we take typical parameters described in Section 2. The comoving radius $R' = 10^{13}$ cm, the initial Thomson optical depth $\tau_0 = 6 \times 10^{-4}$ (close to the critical τ_{cr}, but higher than τ_{ext}), the compactness $\ell = 3$ (corresponding to $\Gamma \approx 130$ for $E_{rad,52} = 1$; see equation 2) and the magnetic compactness $\Lambda_B = 0.3$ (corresponding to the comoving magnetic field $B' \sim 1000$ G, three times below the equipartition). The evolution of broad-band spectra and electron distributions is shown in Fig. 2.

At the start of simulations $\tau_T = \tau_0 < \tau_{cr}$ and the electron heating and cooling are balanced at high γ (see dashed curves). Partially self-absorbed synchrotron radiation (solid curves, lower energy bump) peaks at $\epsilon_s \sim 3 \times 10^{-7}$ in the comoving frame and has a hard low-energy tail $F_E \propto E^2$ (Ghisellini & Svensson 1991). The optical depth grows nearly linearly with time due to electron–positron pair

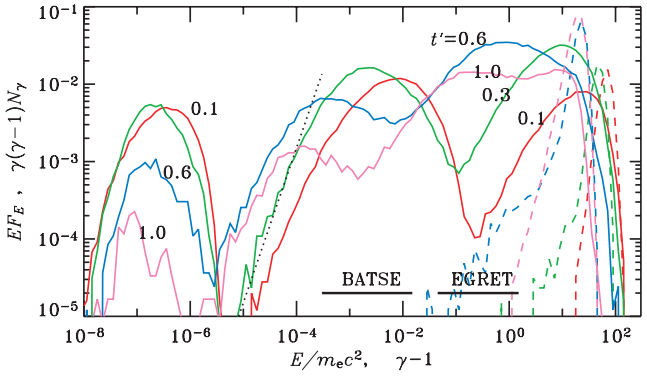

Figure 2. Instantaneous (comoving frame) photon spectra within the slab (i.e. the source functions) and corresponding electron distributions. The solid curves show the photon spectra EF_E (in arbitrary units) at times of 0.1, 0.3, 0.6 and 1 (in units R'/c). The spectra consist of a low-energy (partially self-absorbed) synchrotron bump and two Compton scattering orders. Further scatterings are suppressed due to the Klein–Nishina effect. The electron energy distribution function $\gamma(\gamma - 1)\,dN/d\gamma$ for the same time intervals is shown by dashed curves (the peak evolves towards lower energies). The parameters of the simulations are $R' = 10^{13}$ cm, $\tau_0 = 6 \times 10^{-4}$, $\ell = 3$ and $\Lambda_B = 0.3$. The dotted line shows the hardest possible $F_E \propto E^1$ power law reachable at the low-energy slope of the first Compton bump. The BATSE (20–1000 keV) and the Energetic Gamma-Ray Experiment Telescope (EGRET, 3–100 MeV) bands redshifted to a comoving frame by $(1 + z)/2\Gamma$ (where $z \sim 1$ is the cosmological redshift and $\Gamma = 130$) are shown by horizontal bars.

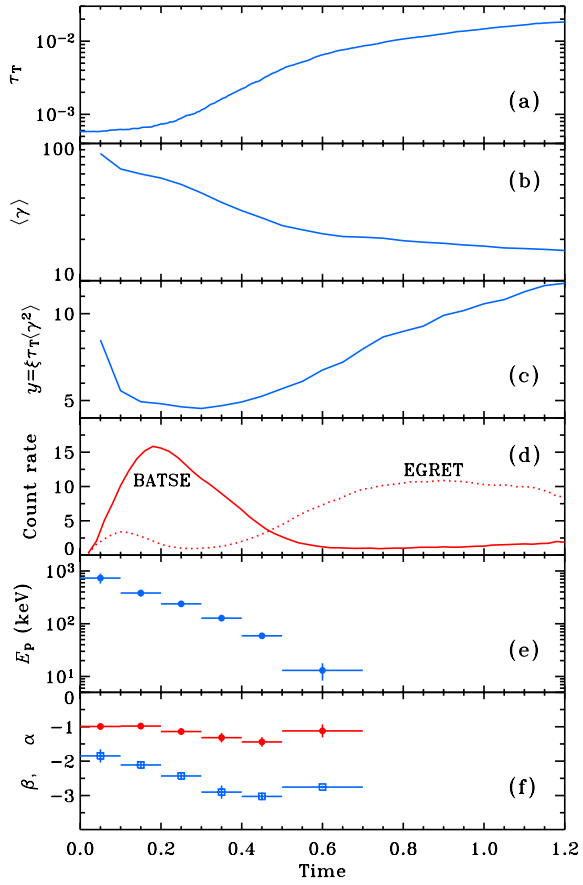

Figure 3. Evolution (a) of the Thomson optical depth due to pair production, (b) of the mean electron Lorentz factor $\langle\gamma\rangle$, and (c) of the Compton y-parameter. (d) Photon flux in the BATSE band (solid curve) and the EGRET band (dotted curve) in arbitrary units. Evolution of spectral parameters (e) E_p, (f) α (circles) and β (squares).

production (see Fig. 3a) and the mean particle energy decreases as $\langle\gamma\rangle \propto 1/\sqrt{\tau}$ (Fig. 3b). The Compton parameter $y = \xi\tau_T\langle\gamma^2\rangle$ computed from the pair distribution (see Fig. 3c) is about 8 in the beginning, reaches minimum at $t' = 0.3$ and grows to more than 10 by the end of energy injection. The 'observed' y-parameter, i.e. the ratio of luminosities in the first Compton bump to the synchrotron component grows monotonically, however, from 3 at $t' = 0.1$ to 16 at $t' = 1$. This discrepancy is caused by the non-stationarity of the problem – it takes too long a time to build up the spectrum and to reach a steady state.

The first Compton peak $\propto\langle\gamma^2\rangle$ moves to softer energies and crosses the 'BATSE window' (note that due to self-absorption, the synchrotron peak energy is very stable). This spectral evolution is consistent with the observed in time-resolved pulses (e.g. Ford et al. 1995; Ryde & Svensson 2002). The photon flux in the BATSE band (Fig. 3d) shows a 'fast rise – exponential decay' behaviour often seen in GRBs. It decays much before the energy supply terminates, but has a long flat part. In contrast, the second Compton peak at ~10–100 MeV rises later and decays on a longer time-scale.

We fitted the model photon spectrum $N_E = F_E/E$ in the BATSE window by a phenomenological 'GRB function' consisting of a power law with an exponential cut-off, $N_E \propto E^\alpha \exp[-E(2 + \alpha)/E_p]$, merging to a high-energy power law $\propto E^\beta$ (Band et al. 1993). The evolution of the fitted (observed) peak energy E_p of the EF_E spectrum and the spectral slopes is shown in Figs 3(e) and (f).

One sees softening of the spectrum as the burst progresses. The fitted α is close to -1, the most probable value in the distribution of time-resolved spectra (Preece et al. 2000). The results of spectral fitting depend somewhat on the used energy interval: α becomes larger (spectrum hardens) in a wider interval and β is softer. Often the data at lower energies (with better statistics) dominate the fitting procedure; then the fitted α can be much harder. A correlation between α and $E_{\rm p}$ is also expected. The hardest possible spectrum, $\alpha = 0$, corresponds to Compton scattering by isotropic monoenergetic electrons (Blumenthal & Gould 1970; Rybicki & Lightman 1979).

4 SUMMARY

The radiative processes that are responsible for particle cooling depend on the optical depth in the emission region. If $\tau_{\rm T}$ is very small, the mean γ is large and the BATSE photons would be produced by synchrotron radiation. At $\tau_{\rm T} \sim 1$, quasi-thermal Comptonization operates. At intermediate $\tau_{\rm T} \sim 3 \times 10^{-4}$–$10^{-2}$, the electrons/pairs have $\gamma \sim 30$–100 and the first Compton peak is produced in the BATSE band. Such optical depth seems natural for the external shock in the typical Wolf–Rayet progenitor wind as well as for the emission within the ejecta (e.g. due to magnetic reconnection or collisions of the fresh ejecta with already decelerated material). Efficient pair production at intermediate compactnesses, $\ell = 0.1$–10, also can be responsible for the required $\tau_{\rm T}$.

Synchrotron self-Compton emission from continuously heated, nearly monoenergetic electrons can explain many observed features of GRBs. The synchrotron spectrum peaking at $\epsilon \sim 3 \times 10^{-7}$ in the comoving frame will be blueshifted to the extreme ultraviolet region. The self-absorbed low-energy tail is hard, $F_E \propto E^2$, and can explain the prompt optical radiation detected from GRB 990123 (Akerlof et al. 1999). The energy of the first Compton peak is expected to decrease as the burst progresses because pair production reduces the mean energy available per particle. In the case of a larger τ_0 and/or a higher compactness and/or a smaller Γ, the first Compton component peaks in X-rays and possibly can be identified with the observed X-ray flashes (e.g. Heise 2003).

The GRB spectral hardness distribution (Preece et al. 2000) can also be reproduced (maybe except its hardest events, see Ghirlanda, Celotti & Ghisellini 2003). Because the incident synchrotron spectrum is hard, the low-energy slope of the scattered radiation, $F_E \propto E^1$, is determined by the kinematics of single Compton scattering by monoenergetic electrons.

The second inverse Compton peak observed at 10 MeV–10 GeV is delayed relative to the soft gamma-ray emission and lasts longer. In spite of the large y-parameter, this peak does not necessarily dominate the total energy output because of the Klein–Nishina effect. The rather hard ($\alpha \sim -1$) spectrum at $\sim$10 MeV can match observations of GRB 941017 (González et al. 2003) and its observed slow evolution. If the mean particle energy decreases rapidly, this component can possibly produce even the second distinct pulse in the BATSE range.

Summarizing, the proposed model can explain a large fraction of GRB spectra and their time evolution. It also reproduces the high-energy $\sim$10–100 MeV emission detected by EGRET in some bursts and the prompt optical emission. These two phenomena are natural within this model and do not require additional assumptions or separate emission regions.

ACKNOWLEDGMENTS

We thank Marek Sikora for useful discussions and suggestions. This research has been supported by the RFBR grant 04-02-16987, Academy of Finland, Jenny and Antti Wihuri Foundation, Vilho, Yrjö and Kalle Väisälä Foundation, and the NORDITA Nordic project in High Energy Astrophysics.

REFERENCES

Akerlof C. et al., 1999, Nat, 398, 400
Band D. L. et al., 1993, ApJ, 413, 281
Beloborodov A. M., Stern B. E., Svensson R., 2000, ApJ, 535, 158
Blumenthal G. R., Gould R. J., 1970, Rev. Mod. Phys., 42, 237
Bussard R. W., 1984, ApJ, 284, 357
Chiang J., Dermer C. D., 1999, ApJ, 512, 699
Ford L. A. et al., 1995, ApJ, 439, 307
Frederiksen J. T., Hededal C. B., Haugbølle T., Nordlund Å., 2003, preprint (astro-ph/0303360)
Ghirlanda G., Celotti A., Ghisellini G., 2003, A&A, 406, 879
Ghisellini G., Celotti A., 1999, ApJ, 511, L93
Ghisellini G., Svensson R., 1991, MNRAS, 252, 313
Ghisellini G., Celotti A., Lazzati D., 2000, MNRAS, 313, L1
González M. M., Dingus B. L., Kaneko Y., Preece R. D., Dermer C. D., Briggs M. S., 2003, Nat, 424, 749
Heise J., 2003, in Ricker G. R., Vanderspek R. K., eds, AIP Conf. Proc. 662, Gamma-ray burst and afterglow astronomy 2001. Am. Inst. Phys., Woodbury, NY, p. 229
Imamura J. N., Epstein R. I., 1987, ApJ, 313, 711
Liang E. P., 1997, ApJ, 491, L15
Lloyd N. M., Petrosian V., 2000, ApJ, 543, 722
Lyutikov M., Blandford R. D., 2003, preprint (astro-ph/0312347)
Panaitescu A., Mészáros P., 2000, ApJ, 544, L17
Piran T., 1999, Phys. Rep., 314, 575
Preece R. E., Briggs M. S., Malozzi R. S., Pendleton G. N., Paciesas W. S., Band D. L., 2000, ApJS, 126, 19
Rees M. J., Mészáros P., 1992, MNRAS, 258, L41
Rybicki G. B., Lightman A. P., 1979, Radiative Processes in Astrophysics. Wiley, New York
Ryde F., Svensson R., 2002, ApJ, 566, 210
Stern B. E., 1985, SvA, 29, 306
Stern B. E., 1999, in Poutanen J., Svensson R., eds, ASP Conf. Sec. Vol. 161, High Energy Processes in Accreting Black Holes. Astron. Soc. Pac., San Francisco, p. 277
Stern B. E., 2003, MNRAS, 345, 590
Stern B. E., Begelman M. C., Sikora M., Svensson R., 1995, MNRAS, 272, 291
Tavani M., 1996, ApJ, 466, 768
Thompson C., 1994, MNRAS, 270, 480
Usov V. V., 1994, MNRAS, 267, 1035
Zdziarski A. A., Lamb D. Q., 1986, ApJ, 309, L79

This paper has been typeset from a TEX/LATEX file prepared by the author.